



All-solution processed, scalable superhydrophobic coatings on stainless steel surfaces based on functionalized discrete titania nanotubes

Partha Roy^{a,e}, Ryan Kisslinger^a, Samira Farsinezhad^a, Najia Mahdi^a, Advaita Bhatnagar^b, Arezoo Hosseini^a, Lintong Bu^a, Weidi Hua^a, Benjamin D. Wiltshire^a, Andrew Eisenhawer^d, Piyush Kar^a, Karthik Shankar^{a,c,*}

^a Department of Electrical and Computer Engineering, University of Alberta, 9211-116 St, Edmonton, Alberta T6G 1H9, Canada

^b Department of Chemical and Materials Engineering, University of Alberta, 9211-116 St, Edmonton, Alberta T6G 1H9, Canada

^c NRC National Institute for Nanotechnology, 11421 Saskatchewan Dr. NW, Edmonton, AB T6G 2M9, Canada

^d WaveControl Systems Inc., Edmonton, AB, Canada

^e Department of Chemistry, Central University of Rajasthan, NH-8, Bandar Sindri, Dist-Ajmer-305817, Rajasthan, India

HIGHLIGHTS

- Formation of superhydrophobic steel surface with contact angle as high as 166°.
- Demonstration of increased corrosion resistance of steel surfaces after treatment.
- Combination of micro-scale and nano-scale surface texturing.
- All-solution-processing based low cost and scalable technique.
- Characterization of steel surfaces using electrochemical impedance spectroscopy.

ARTICLE INFO

Keywords:

Superhydrophobic surface coating
Discrete TiO₂ nanotubes
Octadecylphosphonic acid (ODPA)
Self-assembled monolayer (SAM)
Corrosion resistance
And stainless steel surfaces

ABSTRACT

Stainless steel structures are used in reactor vessels, pipelines, boilers and industrial tubing in the oil and gas industries and they regularly experience corrosion, erosion and fouling that necessitate frequent replacement and repairs. We demonstrate a new method to robustly protect the stainless steel surface and render it superhydrophobic. Our method utilizes self-assembled monolayers (SAMs) of octadecylphosphonic acid (ODPA) grown on discrete TiO₂ nanotube (d-TNT)-coated stainless steel surfaces for complete passivation. While the formation of superhydrophobic coatings based on anodically formed titania nanotube arrays has been previously reported by several research groups including us, the key techno-economic obstacle has been the need to use vacuum deposition to grow adherent and uniform precursor Ti films on non-native substrates such as stainless steel prior to electrochemical anodization. Vacuum deposition of the precursor Ti films is simply neither scalable nor economically feasible for the large and complex stainless steel structures used in pipelines, boilers and industrial tubing and solution processing, preferably a spray-coatable solution, is an absolute must. Our innovation here consists of formulating a spray-coatable suspension of functionalized discrete TiO₂ nanotubes that forms a superhydrophobic surface on stainless steel substrates. Vacuum deposition is completely eliminated from our process sequence and as such, we expect our coatings to inhabit the same niche as current commercial formulations while possessing the superior temperature stability and wear resistance of TiO₂.

1. Introduction

Stainless steel is one of the most widely used corrosion resistant structural materials in the industrial age. Stainless steel is used in the construction of boilers, heat exchangers, reaction vessels and other large scale industrial components. Despite stainless steel's relative

resistance to corrosion, it is nevertheless subject to scale formation, organic fouling, and corrosion, which over time result in pits or weakened structural integrity, loss of thermal conductivity, viscous drag, etc [1]. Increased viscous drag (in pipelines for instance) and lower thermal conductivity (in boilers and heat exchangers) due to scale formation and fouling can dramatically increase energy costs [2,3]

* Corresponding author at: Department of Electrical and Computer Engineering, University of Alberta, 9211-116 St, Edmonton, Alberta T6G 1H9, Canada.
E-mail address: kshankar@ualberta.ca (K. Shankar).

while corrosion of stainless steel surfaces produces additional expenses associated with process downtime, and component repair and replacement [4]. The formation of robust and durable superhydrophobic surfaces would alleviate corrosion and scaling problems by inhibiting the direct interaction of ions in aqueous media with stainless steel surfaces, and therefore remains a highly sought-after goal.

Commercially available superhydrophobic coatings such as formulations based on polytetrafluoroethylene (PTFE) or related systems exhibit strong chemical inertness but are not cost effective for large scale industrial applications. PTFE-based coatings also exhibit poor wear resistance (Teflon is easily eroded) and typically have poor adhesion to steel surfaces [5]. In order to address this problem, extensive research was devoted to protect the steel or stainless steel surface through the formation of self-assembled monolayers (SAMs) with different binding groups [6–9] using non-fluorinated molecules, and cost effective processes and coatings; however, most of the coatings suffered from the hydrolytic instability of the monolayer [10]. Consequently, the best static contact angle (SCA) achieved was 108° [10]. To address this issue, a notable research effort from Fujishima et al. reported superhydrophobic behavior on a bendable stainless steel surface [11], wherein they used sulfuric acid for etching the stainless steel surface and subsequently achieved a hydrophobic surface by silane treatment. The major problem with this approach is that organic monolayers by themselves will always experience significant erosion rates due to which a chemically inert ceramic host coating for the monolayer is essential. Keeping this in mind, in another study, a clean FeCl_3 -treated stainless steel surface was covered with silica nanoparticles followed by the formation of a conformal layer of fluorooxysilane SAM, which imparted a very high static contact angle (SCA) to the stainless steel surface [12]. Yet another method formed Ti thin films on steel surfaces, and then decorated the resulting surfaces with perfluorodecyltriethoxysilane functionalized TiO_2 and SiO_2 nanoparticles to form superhydrophobic steel surfaces [13]. The large area deposition of Ti thin films on stainless steel surfaces is not feasible. Furthermore, nanostructuring the stainless steel surface is insufficient to ensure a durable coating since turbulent flows ($\text{Re} > 4000$) can produce wetting of previously superhydrophobic surfaces within minutes. A more robust method of imparting durable superhydrophobicity is to engineer the formation of Cassie-Baxter type wetting states through a combination of microscale and nanoscale texturing of the surface so that trapped air is present at different size scales to resist water imbibition. However, texturing large area stainless steel surfaces or the insides of stainless steel tubing, is non-trivial. The technique we propose consists of solution depositing functionalized discrete metal oxide nanotubes on stainless steel surfaces to form a coating such that the chemical functionalization imparts water-repellence while the combination of micro- and nano-structuring due to nanotubes facilitates the formation of Cassie-Baxter type wetting states.

We used an electrochemical anodization process to generate a vertically oriented and self-organized array of titania nanotubes (TNTAs) attached to the underlying Ti foil substrate. The morphological parameters of the TiO_2 nanotube architecture such as the diameter, wall-thickness, wall smoothness, tube-length, inter-tubular spacing, aspect ratio and taper, are fairly precisely tunable in a very wide range by careful selection of the anodization process parameters [14–23]. The vast potential of such substrate-attached and highly ordered TNTAs in engineering well-defined wetting states such as superhydrophobicity, superoleophobicity, omniphobicity and adjoining superhydrophilic-superhydrophobic micropatterns through functionalization of TNTAs by alkylphosphonate and perfluoroalkylphosphonate SAMs, have been reported by us and others [24–28]. The formation of functionalized TNTAs has been extended to a number of platforms other than Ti metal foils such as plastic substrates, glass substrates, silicon wafers and even stainless steel substrates through vacuum deposition of a thin film of Ti followed by electrochemical anodization [29–33]. Q. Huang et al. formed superhydrophobic TiO_2 -nanotube-coated 316L stainless steel

surfaces by vacuum depositing Ti on to stainless steel surfaces, anodizing the Ti to form nanotubes and then functionalizing the high surface area TNTAs with 1H,1H,2H,2H-perfluorooctyl-triethoxysilane [34]. However, vacuum deposition of Ti thin films is simply neither technologically nor economically feasible for complex stainless steel components with intricate features, curved surfaces and large physical dimensions. Here, we present a superior approach based purely on solution processing that entirely eliminates the need for vacuum deposition.

In our process, the nanotube array formed by anodization is delaminated from the Ti surface and first converted into a colloidal suspension of discrete titania nanotubes (d-TNTs) through an ultrasonication process, and it is these d-TNTs that are used subsequently by us to coat stainless steel substrates. To overcome limitations of the current state-of-the-art, we herein introduce an elegant method characterized by process simplicity and cost-effectiveness, to coat d-TNTs onto stainless steel surfaces. Our method involves a simple drop-coating of d-TNTs onto the stainless steel surface, which is easily scalable to large stainless steel sheets and even curved surfaces. We obtained impressive SCA and wear resistance, and this is to the best of our knowledge the first report on the use of anodically formed d-TNTs for surface engineering of stainless steel for enhanced corrosion resistance. We chose TiO_2 nanotubes because of their desirable properties such as chemical stability and adaptability to the formation of self-assembled monolayers. Our method to inhibit corrosion, which involves combining d-TNTs and suitable alkylphosphonate or perfluoroalkylphosphonate SAMs, constitutes a cost-effective and robust solution to engineer superhydrophobic stainless steel surfaces.

2. Experimental

2.1. Sample preparation

A 0.5 mm thick stainless steel substrate (T-304 Stainless from McMaster Carr) was used in our experiments. The substrates were initially cleaned by sequential ultrasonication in methanol (99.8%, from Fisher Scientific) then *n*-hexane (99%, from Acros) followed by isopropyl alcohol (99.8%, from Fisher Scientific); 15 min in each solvent. Finally, the cleaned surfaces were treated with O_2 plasma for 10 min in order to get rid of adsorbed carbon impurities. Thereafter, a discrete TiO_2 nanotube (d-TNT) solution was drop-coated on an O_2 plasma treated stainless steel surface and was allowed to be dry overnight. Subsequently, the stainless steel surface coated with d-TNTs was immersed in a 1 mM octadecylphosphonic acid (ODPA) (purchased from Alfa Aesar with 97% purity) solution in 4:1 methanol:water at room temperature for 20 h; alternatively, 1H,1H,2H,2H-perfluorodecylphosphonic acid (PFDDPA) purchased from Aculon Inc. was used in an identical manner to ODPA to generate the samples used for mechanical testing. The as-modified and passivated stainless steel surface was rinsed with methanol in order to remove all physisorbed molecules and dried with N_2 gas flow.

2.2. Formation of d-TNTs

Titanium foils with 0.79 mm thickness (99.7%; Alfa Aesar) were degreased by sonication in methanol and deionized water (DI) and then dried with nitrogen gas. A conventional two-electrode electrochemical cell was used for anodic formation of TiO_2 nanotubes (TNTs) with dimensions of 1×4 cm and 0.5×4 cm for anode and cathode, respectively. An anodizing voltage of 60 V was used. The duration of the anodization was 3 days. An electrolyte consisting of 2% HF and dimethyl sulfoxide (DMSO) was used to form TNTs with weak tube-to-tube binding as well as a weak adhesion to the barrier layer. Hence the substrate delamination and discretization of DMSO-synthesized TiO_2 nanotubes was rendered easier [35]. The as-prepared DMSO-synthesized TNTs were annealed at 500°C in the presence of air for 2 h

[35,36]. The annealed TNTs from one anodized titanium foil (front and back) were detached with a blade into small vials filled with methanol (1 mL in volume). A tip sonicator was used to discretize the TNTs into a colloidal suspension of d-TNTs in methanol. The sonication was started at 150 W amplitude for 4 min and continued at 240 W amplitude for 1 min.

2.3. Electrochemical impedance spectroscopy

Electrochemical impedance spectroscopy (EIS) experiments were performed in 0.1 M supporting electrolyte with a carbon counter electrode and an Ag/AgCl reference electrode. Four samples were analyzed in separate experiments and were used as the working electrode in EIS experiments – these were a bare stainless steel foil, a stainless steel foil coated with an ODPa monolayer, and two stainless steel surfaces coated with discrete TiO₂ nanotubes (d-TNTs) one with and the other without the ODPa SAM. The working electrodes had an area of 1 cm² exposed to electrolyte and the remainder of the area was covered with parafilm. Alternating current (AC) impedance measurements were performed using a CH Instruments potentiostat in the frequency range 0 and 5000 Hz, at potentials near the open circuit potentials of the electrodes.

2.4. Characterization

A Hitachi S-4800 field emission scanning electron microscope (FESEM) and a Zeiss Sigma FESEM were used to image the morphology of the samples. Raman spectra were obtained using a Thermo-Fisher Scientific Nicolet Almega XR micro-Raman spectrometer Thermo-Fisher Scientific. Infrared spectra were obtained using a Thermo Scientific IR spectrometer. A First Ten Angstroms Inc. FTA-200 water drop contact angle measurement system together with ImageJ software, was used to make SCA measurements.

2.5. Wear resistance and adhesion testing

Wear resistance testing of the coating was conducted by the sandpaper abrasion method, where a stainless steel sample was placed on 320 grit sandpaper with the coating facing downwards [37,38]. A 50 g weight was placed on top of the sample, and the sample then pushed horizontally with a pair of tweezers for 5 cm increment cycles, with water drop contact angle measured in between each abrasion cycle. Adhesion of the coating was evaluated by a tape test using Elcometer 99 Cross Hatch Adhesion Test Tape and following ASTM D3359 – 17 [39], except for modifications during adhesion evaluations (reasoning is explained later). In brief, a blade was used to scratch 5 parallel cuts 20 mm long spaced 1 mm apart in the coating, followed by another 5 cuts identical to the first 5 except perpendicular in orientation to produce a lattice pattern. The tape was pressed down firmly, left for one minute, and then pulled off quickly. The coating before and after the tape test was compared by FESEM, and the resultant images processed using ImageJ.

3. Results and discussion

The process for coating stainless steel surfaces with d-TNTs and subsequently with octadecylphosphonic acid (ODPA) SAMs is schematically described in Fig. 1. Briefly, d-TNTs were drop-coated on to pre-cleaned stainless steel foils to generate a several micrometer-thick white, porous coating on the stainless steel surface. The pre-existing negative charge on the d-TNTs, as a consequence of the process used to grow them, created a strong electrostatic interaction with the stainless steel surface such that the porous film that resulted after drop-coating the d-TNTs on the stainless steel surface resisted repeated and strong washing and rinsing cycles in water as well as subsequent drying using a nitrogen gun. The porous coating on the stainless steel surface was then immersed in a 4:1 methanol:water solution of ODPa in order to

form hydrophobic self-assembled ODPa monolayers on all exposed metal (stainless steel) and metal oxide (TiO₂) surfaces. This process exploits the well-established affinity of the phosphonic acid functional group for metal and metal oxide surfaces [40–46]. Indeed, phosphonate head group containing molecules are used as components in commercially used corrosion inhibitors for stainless steel surfaces [47,48]; however these molecules fulfill other functions such as transporting sacrificial agents to the stainless steel surface and typically do not form well-ordered and durable monolayers on the stainless steel surface due to which the concentration of inhibitors on the stainless steel surface typically need to be periodically replenished. Nanostructured metal oxides, such as TiO₂ nanotubes, are superior to bare metal surfaces in that they minimize the contact area, and as a result, achieve a higher SCA [26,49,50]. The nanotubes exhibit a low contact area fraction parameter and contain pockets of trapped air within the nanotubes. The solution deposition of d-TNTs on the stainless steel surface also creates micro-scale voids in between the nanotubes. The combination of d-TNTs and ODPa SAMs, according to Cassie-Baxter model [51], is expected to render the stainless steel surface superhydrophobic, as illustrated in Fig. 1 (4).

The Raman spectrum (Fig. 2) of d-TNT coated stainless steel surfaces confirmed the crystalline anatase phase of the d-TNTs along with the possible presence of a small amount of the brookite phase [52,53]. Annealing the nanotubes prior to their delamination from the Ti foil substrate also ensured stoichiometric d-TNTs with undesirable impurities such as fluoride species greatly reduced (please note that fluoride species were considered undesirable because of our desire to maximize the strong and stable P-O-Ti bonds that form [54], although to the best of our knowledge the effect of fluoride species on SAMs formation on TiO₂ is yet to be studied). Fig. 3 shows the dramatic change in visual appearance of the stainless steel substrate after coating with d-TNTs. In Fig. 3a, the initially dark stainless steel substrate on the left turns completely white due to the d-TNT coating. The white appearance is a consequence of the broadband Mie scattering from the assembly of discrete titania nanotubes. The open circuit potentials of the electrodes were determined by Tafel analysis (Fig. 3b), and are the potentials at zero current. The 0.25 V negative shift in the open circuit potential for the stainless steel substrate following d-TNT coating and subsequent ODPa functionalization demonstrates the passivation and improved corrosion resistance of the stainless steel substrate [7].

The morphology of d-TNT incorporated stainless steel surfaces was characterized by field emission scanning electron microscopy (FESEM). As shown in Fig. 4(a), d-TNTs maintain the nanotubular morphology after adherence onto the stainless steel surface. The inset is a higher magnification FESEM image of d-TNTs incorporated on the stainless steel surface depicting the dimensional details of individual d-TNTs. Diameters of the nanotubes were 100–150 nm and tube lengths were 8–12 μm resulting in an aspect ratio of 50–120. The hollow cylindrical structure of the nanotubes ensures the presence of sub-micrometer scale voids while the tube-lengths and spacing between the nanotubes creates micro-scale voids. Mie scattering is a phenomenon that requires the presence of micrometer-scale features to resonantly scatter photons. The broadband optical Mie scattering evident in Fig. 3a (right) provides confirmation of micro-scale texturing of the stainless steel surface over a large area.

In infrared reflection absorption spectroscopy (IRRAS) measurement, two distinct peaks appeared at 2917 cm⁻¹ and 2849 cm⁻¹, which were attributed to CH₂ anti-symmetric and symmetric stretching modes, respectively (Fig. 4c) [55]. The presence of the phosphonate group was confirmed by two peaks, which are ν_{P-O} (~1050 cm⁻¹) and ν_{P=O} (~1150 cm⁻¹) (Fig. 4d). Additionally, these findings showed no sign of ν_{P-O-H} = 920 cm⁻¹ (Fig. 4d), indicating a bidentate coordination mode of the phosphonate to the surface [10]. According to the literature, the position of the CH₂ anti-symmetric peak is a measure of the organization of the monolayer on the surface. If the CH₂ anti-symmetric peak appears below 2920 cm⁻¹ the monolayer may be considered as a

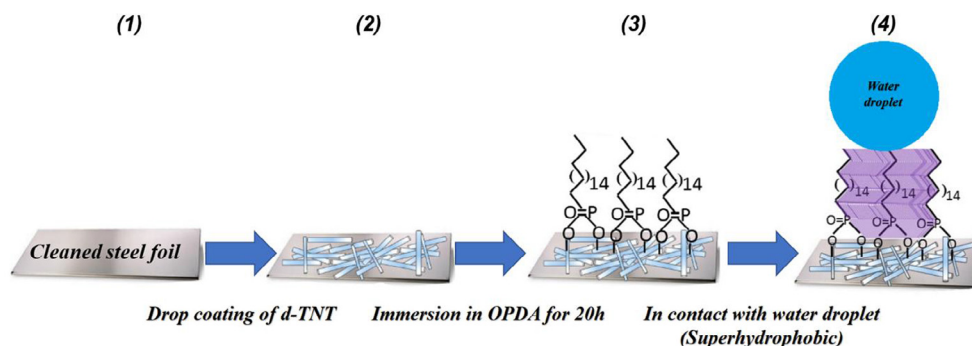


Fig. 1. Stepwise schematic representation of passivation of the stainless steel surface (2–3) and illustration of the expected superhydrophobic behavior of passivated stainless steel surfaces (4).

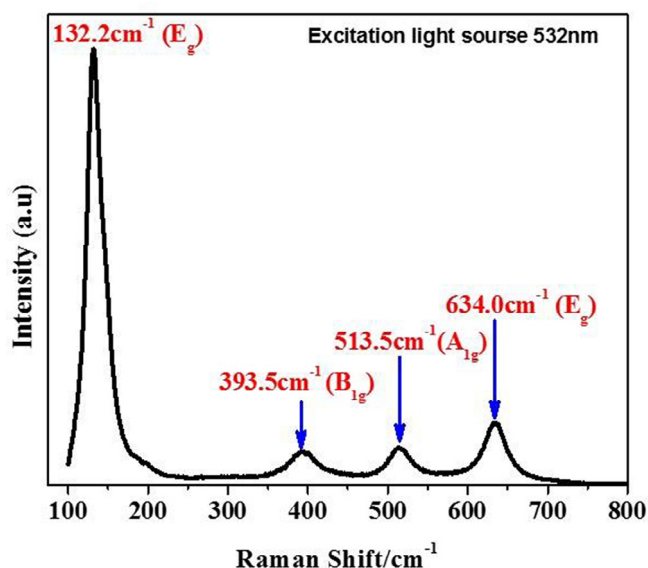


Fig. 2. Raman spectrum of TiO₂ nanotubes, excited by a 532 nm laser.

well-ordered monolayer (qualitatively) on the surface [56]. Therefore, the IR peak position of 2917 cm⁻¹ for CH₂ anti-symmetric stretching (Fig. 4c) demonstrates the formation of a well-ordered monolayer of OPDA on the d-TNT coated stainless steel surface.

Quantification of the surface coverage of the OPDA SAMs over d-TNTs was performed using electrochemical impedance spectroscopy (EIS). Fig. 4b shows the Nyquist plots for the stainless steel surface under various conditions. The total impedance of the system, as illustrated by the equivalent circuit (Fig. 5), was fitted to experimental data to extract the circuit parameters. Fig. 5a is the equivalent circuit for bare stainless steel and stainless steel with the OPDA SAM, and Fig. 5b is the equivalent circuit for stainless steel with d-TNTs and stainless steel with d-TNTs as well as OPDA SAM. R_s is the electrolyte resistance, C_D is the electrochemical double layer capacitance, R_c is the charge transfer resistance, Q is a constant phase element associated with the system, and n is the exponent of the constant phase element. These equivalent circuit parameters are tabulated in Table 1. Surface coverage (θ) was calculated using Eq. (1) [57]. The obtained value of θ was 75% for stainless steel with d-TNTs and OPDA SAM, whereas the same for stainless steel with ML was 99%.

$$\theta = 1 - \frac{R_c(\text{without ML})}{R_c(\text{with ML})} \quad (1)$$

Nyquist plots (Fig. 4b) were obtained from electrochemical impedance spectroscopy (EIS), and show different characteristics for bare stainless steel, stainless steel with d-TNT, stainless steel with d-TNT and

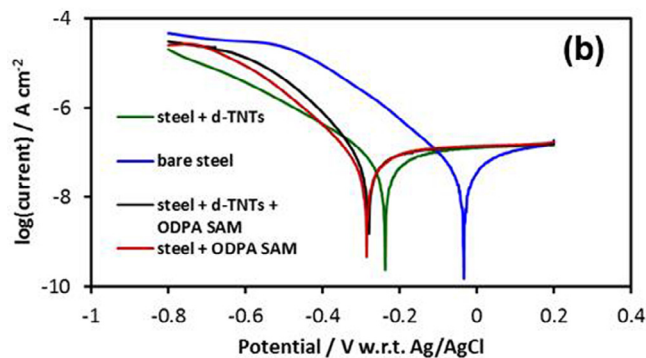
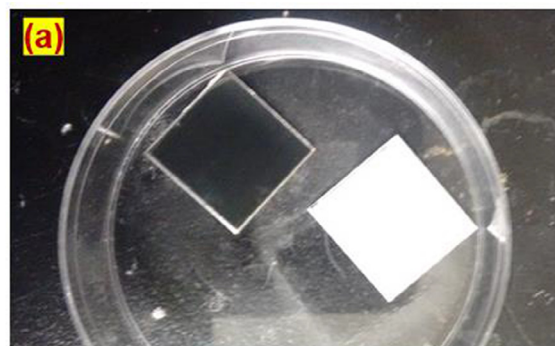


Fig. 3. (a) Photographs of the stainless steel substrate before (left) and after (right) coating with d-TNTs and (b) Tafel plots for bare stainless steel (blue), stainless steel with OPDA SAM (red), stainless steel with d-TNTs (green) and stainless steel with d-TNTs and OPDA SAM (black). (For interpretation of the references to color in this figure legend, the reader is referred to the web version of this article.)

OPDA SAM, and stainless steel with OPDA SAM. Stainless steel with the OPDA SAM exhibits the largest impedance in absolute value and the bare stainless steel exhibits the smallest impedance. The plot for stainless steel with d-TNT is similar to the stainless steel with OPDA SAM except that the capacitive impedance (with contributions from C_D and Q) is more pronounced in d-TNT without OPDA SAM. The values of capacitances and resistances, obtained by fitting the experimental Nyquist plots with transfer function of total impedances show that the charge transfer resistances, R_c , of stainless steel with TNTs as well as OPDA SAMs is 200 ohms and the stainless steel/d-TNTs without OPDA SAM is 50 ohms. Similarly, R_c of stainless steel with OPDA is 20,000 ohms as compared to 75 ohms for bare stainless steel. Surface coverage of the OPDA SAM, was quantified by using the charge transfer resistances, and is 75% for stainless steel with d-TNTs and OPDA SAM, and 99% for stainless steel with OPDA SAM (and without d-TNTs). It is

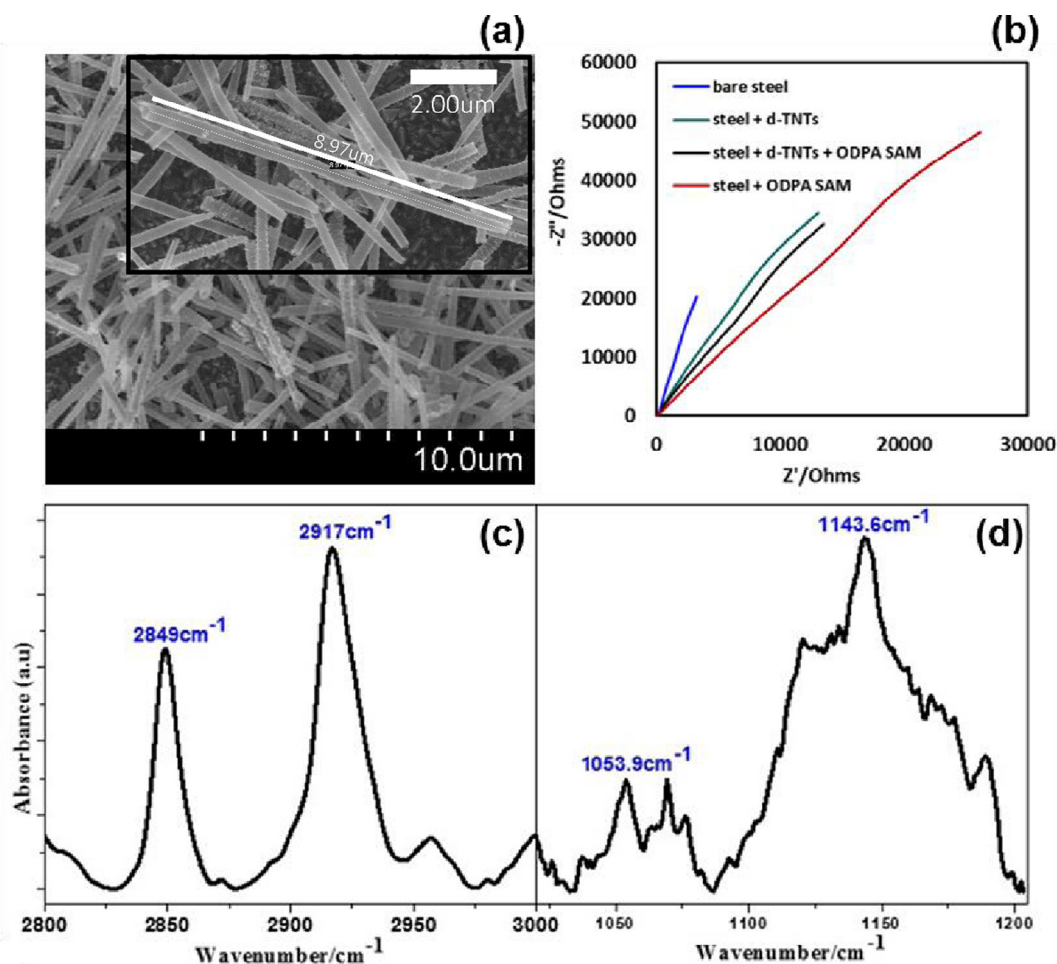


Fig. 4. (a) FESEM images of the discrete TiO_2 nanotubes on the stainless steel surface; (b) EIS Nyquist plots for bare stainless steel, stainless steel with ODPA SAM, stainless steel with d-TNTs and stainless steel with d-TNTs and ODPA SAM; IR spectra of C–H stretching and P–O stretching regions of ODPA monolayer are shown in (c) and (d), respectively.

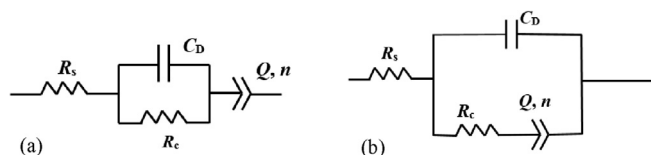


Fig. 5. Equivalent circuit representing bare stainless steel and stainless steel with SAM (a), and the same for stainless steel with d-TNT as well as stainless steel with d-TNT and SAM (b).

noteworthy that 75% surface coverage led to an impressive SCA. Considering that various factors, including nanotube aspect ratio and SAM formation process, can affect the extent and quality of surface coverage, there is room for optimization of the ODPA SAM monolayer in order to further improve performance of the coating.

After formation of the ODPA SAMs, we systematically investigated

the SCA of bare stainless steel, stainless steel coated with the ODPA SAM, stainless steel coated with d-TNTs, and stainless steel coated with d-TNTs as well as the ODPA SAM. We performed the SCA measurements by dropping 4 μL of water onto the stainless steel surface. The SCA for O_2 plasma treated stainless steel surface was $ca. 20^\circ$ (Fig. 3a) which indicates it to be strongly hydrophilic. The ODPA coated stainless steel surface exhibited a contact angle of $111 \pm 2^\circ$ (Fig. 6b) and this value is in good agreement with literature [10]. The d-TNT coated stainless steel exhibited a SCA value of $39 \pm 2^\circ$ (Fig. 6c). However, the stainless steel surface with d-TNTs and ODPA SAMs had a remarkably improved SCA of $166 \pm 8^\circ$ (Fig. 6d), which was our expectation as illustrated in Fig. 1. We demonstrate that O_2 plasma cleaned stainless steel, exhibiting consistent superhydrophilicity, becomes superhydrophobic after our d-TNT and ODPA SAM treatment. The resilience of stainless steel surfaces passivated by d-TNTs and ODPA SAMs to turbulent aqueous media is qualitatively demonstrated under water stream flow

Table 1

EIS generated values of circuit elements of bare stainless steel, stainless steel with ODPA SAM, stainless steel with d-TNTs, and stainless steel with d-TNTs and ODPA SAM.

	R_s (ohms)	C_D (F)	R_c (ohms)	Q ($\text{S}\cdot\text{s}^n$)	n
Bare stainless steel (O_2 plasma treated)	75	1.00×10^{-7}	75	1.12×10^{-5}	0.925
Stainless steel + ODPA SAM	75	1.15×10^{-5}	20,000	4.00×10^{-6}	0.690
Stainless steel + d-TNTs	75	3.00×10^{-7}	50	6.00×10^{-6}	0.800
Stainless steel + d-TNTs + ODPA SAM	75	7.00×10^{-6}	200	7.00×10^{-6}	0.760

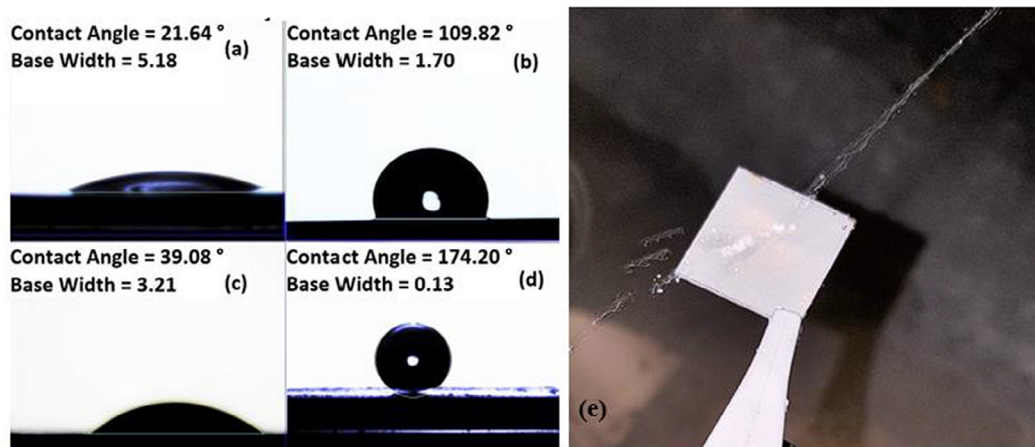


Fig. 6. Static contact angle values for (a) O₂ plasma cleaned stainless steel surface (b) ODPa coated stainless steel surface (c) d-TNT passivated stainless steel surface and (d) ODPa coated d-TNTs on stainless steel surface (e) Photograph of water jet impacting the stainless steel surface coated with d-TNTs and the ODPa SAM.

from a wash bottle (Fig. 6e). We continued the water stream impact process for several minutes and observed that the water rebounds up and around upon contacting the surface with no changes occurring over a 10 min span.

Wear resistance was evaluated by the sand abrasion method [58,59], measuring the SCA of samples as it changed with increasing amounts of abrasion, as shown in Fig. 7a. For this testing, stainless steel coated with d-TNAs using PFDPA SAMs were used. PFDPA-based samples achieved lower contact angles than their ODPa counterparts (as evidenced by Fig. 7a at 0 cm abrasion length), but nevertheless generated superhydrophobic surfaces. More importantly, the PFDPA d-TNT coatings appeared to exhibit identical mechanical properties as ODPa d-TNT coatings during handling. Looking again at Fig. 7a, the results suggest a decrease in SCA as the amount of abrasion increased; however, the much larger spread in contact angles between locations on the sample (reflected in the figure as the larger standard deviation) is also interesting. The SCA values of the sample before abrasion testing (shown as 0 cm in the figure) were so close in value that the error bars in the figure cannot be seen at the scale shown; that they proceeded to increase suggests that the wear resistance of the coating across the sample may not be uniform. One further caveat must be mentioned: we noticed that approximately 10% of the coating was removed entirely by the abrasion testing at the 15 cm abrasion length mark. The SCA of

these spots was measured to be $127 \pm 1^\circ$, but did not include this in the spots evaluated as part of Fig. 7a, as they were so heterogeneously different. We also evaluated the adhesion of ODPa coated d-TNT coatings using a tape test method. As mentioned earlier, the test largely followed the ASTM D3359 – 17 with a modification. After removal of the tape, we did not notice flaking or chipping as is described in the standard, but instead noticed the color of the sample shift from the stark white associated with a thick, more continuous coating to a whitish-grey associated with a thinner, less continuous one. Thus, FESEM images were acquired before and after removal of the tape, as shown in Fig. 7b and c. Clearly, significant amounts of the coating were removed by the tape test and analysis of these FESEM images suggests a 80% loss of the coating. It can be surmised that there is room for improvement in the adhesion of the d-TNT to the substrate.

4. Conclusion

A new strategy is demonstrated to completely render a stainless steel surface superhydrophobic via solution processing methods, a method to increase the corrosion resistance of a superhydrophobic stainless steel surface. Hallmarks of the method are process simplicity, scalability, and cost effectiveness. This robust and wear resistant superhydrophobic coating on stainless steel surfaces uses anodically

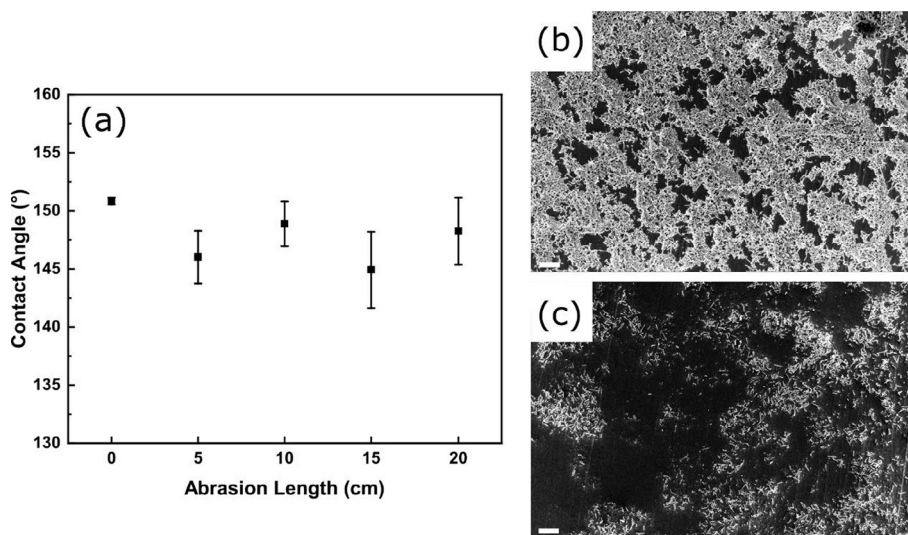


Fig. 7. (a) Static contact angle measurements of a PFDPA coated d-TNTs on stainless steel with corresponding abrasion length over sandpaper. FESEM images before and after a tape adhesion test of ODPa coated d-TNT coatings on stainless steel are shown in (b) and (c) respectively.

formed discrete TiO₂ nanotubes and ODPa SAMs. The industrial significance of this method is emphasized by the fact that a contact angle of $166 \pm 8^\circ$ was obtained for stainless steel surfaces passivated by d-TNTs and ODPa SAM, implying highly water repellent behavior and corrosion resistance. This coating may be able to be extended to other substrates although we make a final note that initial trials depositing our d-TNTs on glass and polystyrene resulted in the formation of island spots rather than full coverage. The extension of the d-TNT/SAMs coatings to other substrates, as well as improving the mechanical properties of the coatings in general comprise potential topics for future work.

Acknowledgments

All authors thank NSERC, CMC Microsystems and NRC-NINT for direct and indirect (equipment use) financial support. S.F. and B.D.W. thank Alberta Innovates for scholarship support.

References

- [1] J. Hernandez, A. Muñoz, J. Genesca, Formation of iron-carbonate scale-layer and corrosion mechanism of API X70 pipeline steel in carbon dioxide-saturated 3% sodium chloride, *Afinidad* 69 (2012).
- [2] L.M. Al-Hadhrani, A. Qudus, D.A. Al-Otaibi, Calcium sulfate scale deposition on coated carbon steel and titanium, *Desalination* 251 (2013) 2521–2528.
- [3] L. Liu, X.F. Guo, Q.Y. Guo, H.Q. Fan, Z.H. Zhong, Drag reduction of gas-liquid two-phase flow in steel pipes with different inclination geometry, *Advanced Materials Research* (2012) 463–470. *Trans Tech Publ.*
- [4] G. Zhang, Y. Cheng, On the fundamentals of electrochemical corrosion of X65 steel in CO₂-containing formation water in the presence of acetic acid in petroleum production, *Corros. Sci.* 51 (2009) 87–94.
- [5] S.K. Biswas, K. Vijayan, Friction and wear of PTFE—A review, *Wear* 158 (1992) 193–211.
- [6] P. Jussila, H. Ali-Löytty, K. Lahtonen, M. Hirsimäki, M. Valden, Effect of surface hydroxyl concentration on the bonding and morphology of aminopropylsilane thin films on austenitic stainless steel, *Surf. Interface Anal.* 42 (2010) 157–164.
- [7] F.S. de Souza, A. Spinelli, Caffeic acid as a green corrosion inhibitor for mild steel, *Corros. Sci.* 51 (2009) 642–649.
- [8] A. Caro, V. Humblot, C. Méthivier, M. Minier, L. Barbes, J. Li, M. Salmain, C.-M. Pradier, Bioengineering of stainless steel surface by covalent immobilization of enzymes. Physical characterization and interfacial enzymatic activity, *J. Colloid Interface Sci.* 349 (2010) 13–18.
- [9] S. Gam-Derouich, S. Mahouch-Chergui, M. Turmine, J.-Y. Piquemal, D.B. Hassen-Chehimi, M. Omastová, M.M. Chehimi, A versatile route for surface modification of carbon, metals and semi-conductors by diazonium salt-initiated photopolymerization, *Surf. Sci.* 605 (2011) 1889–1899.
- [10] N.S. Bhairamadgi, S.P. Pujari, F.G. Trovela, A. Debrassi, A.A. Khamis, J.M. Alonso, A.A. Al Zahrani, T. Wennekes, H.A. Al-Turaif, C. van Rijn, Hydrolytic and thermal stability of organic monolayers on various inorganic substrates, *Langmuir* 30 (2014) 5829–5839.
- [11] S.S. Lathe, P. Sudhagar, A. Devadoss, A.M. Kumar, S. Liu, C. Terashima, K. Nakata, A. Fujishima, A mechanically bendable superhydrophobic steel surface with self-cleaning and corrosion-resistant properties, *J. Mater. Chem. A* 3 (2015) 14263–14271.
- [12] L.B. Boinovich, A.M. Emelyanenko, V.K. Ivanov, A.S. Pashinin, Durable icephobic coating for stainless steel, *ACS Appl. Mater. Interfaces* 5 (2013) 2549–2554.
- [13] T.T. Isimjan, T.Y. Wang, S. Rohani, A novel method to prepare superhydrophobic, UV resistance and anti-corrosion steel surface, *Chem. Eng. J.* 210 (2012) 182–187.
- [14] G.K. Mor, O.K. Varghese, M. Paulose, N. Mukherjee, C.A. Grimes, Fabrication of tapered, conical-shaped titania nanotubes, *J. Mater. Res.* 18 (2003) 2588–2593.
- [15] G.K. Mor, K. Shankar, M. Paulose, O.K. Varghese, C.A. Grimes, Enhanced photocleavage of water using titania nanotube arrays, *Nano Lett.* 5 (2005) 191–195.
- [16] M. Paulose, K. Shankar, S. Yoriya, H.E. Prakasham, O.K. Varghese, G.K. Mor, T.A. Latempa, A. Fitzgerald, C.A. Grimes, Anodic growth of highly ordered TiO₂ nanotube arrays to 134 μm in length, *J. Phys. Chem. B* 110 (2006) 16179–16184.
- [17] H.E. Prakasham, K. Shankar, M. Paulose, O.K. Varghese, C.A. Grimes, A new benchmark for TiO₂ nanotube array growth by anodization, *J. Phys. Chem. C* 111 (2007) 7235–7241.
- [18] K. Shankar, G.K. Mor, A. Fitzgerald, C.A. Grimes, Cation effect on the electrochemical formation of very high aspect ratio TiO₂ nanotube arrays in formamide – Water mixtures, *J. Phys. Chem. C* 111 (2007) 21–26.
- [19] J.M. Macák, H. Tsuchiya, P. Schmuki, High-Aspect-Ratio TiO₂ Nanotubes by Anodization of Titanium, *Angew. Chem. Int. Ed.* 44 (2005) 2100–2102.
- [20] J.M. Macák, H. Tsuchiya, L. Taveira, S. Aldabergerova, P. Schmuki, Smooth Anodic TiO₂ Nanotubes, *Angew. Chem. Int. Ed.* 44 (2005) 7463–7465.
- [21] A. Mohammadpour, K. Shankar, Anodic TiO₂ nanotube arrays with optical wave-length-sized apertures, *J. Mater. Chem.* 20 (2010) 8474–8477.
- [22] S. Yoriya, Effect of inter-electrode spacing on electrolyte properties and morphologies of anodic TiO₂ nanotube array films, *Int. J. Electrochem. Sci* 7 (2012) 9454–9464.
- [23] D. Kowalski, J. Mallet, J. Michel, M. Molinari, Low electric field strength self-organization of anodic TiO₂ nanotubes in diethylene glycol electrolyte, *J. Mater. Chem. A* 3 (2015) 6655–6661.
- [24] S. Nishimoto, Y. Sawai, Y. Kameshima, M. Miyake, Underwater superoleophobicity of TiO₂ nanotube arrays, *Chem. Lett.* 43 (2014) 518–520.
- [25] P. Tang, W. Zhang, Y. Wang, B. Zhang, H. Wang, C. Lin, L. Zhang, Effect of superhydrophobic surface of titanium on *Staphylococcus aureus* adhesion, *J. Nanomater.* 2011 (2011) 2.
- [26] S. Farsinezhad, P.R. Waghmare, B.D. Wiltshire, H. Sharma, S. Amiri, S.K. Mitra, K. Shankar, Amphiphobic surfaces from functionalized TiO₂ nanotube arrays, *RSC Adv.* 4 (2014) 33587–33598.
- [27] S. Farsinezhad, P. Waghmare, B.D. Wiltshire, S. Amiri, S.K. Mitra, K. Shankar, The wetting behavior of TiO₂ nanotube arrays with perfluorinated surface functionalization, *ASME 2014 International Mechanical Engineering Congress and Exposition, American Society of Mechanical Engineers*, 2014, pp. V009T012A071–V009T012A071.
- [28] Y. Lai, C. Lin, H. Wang, J. Huang, H. Zhuang, L. Sun, Superhydrophilic-superhydrophobic micropattern on TiO₂ nanotube films by photocatalytic lithography, *Electrochem. Commun.* 10 (2008) 387–391.
- [29] G.K. Mor, O.K. Varghese, M. Paulose, C.A. Grimes, Transparent highly ordered TiO₂ nanotube arrays via anodization of titanium thin films, *Adv. Funct. Mater.* 15 (2005) 1291–1296.
- [30] V. Galstyan, A. Vomiero, I. Concina, A. Braga, M. Bristotto, E. Bontempi, G. Faglia, G. Sberveglieri, Vertically aligned TiO₂ nanotubes on plastic substrates for flexible solar cells, *Small* 7 (2011) 2437–2442.
- [31] S. Farsinezhad, A. Mohammadpour, A.N. Dalrymple, J. Geisinger, P. Kar, M.J. Brett, K. Shankar, Transparent anodic TiO₂ nanotube arrays on plastic substrates for disposable biosensors and flexible electronics, *J. Nanosci. Nanotechnol.* 13 (2013) 2885–2891.
- [32] S. Farsinezhad, A.N. Dalrymple, K. Shankar, Toward single-step anodic fabrication of monodisperse TiO₂ nanotube arrays on non-native substrates, *Phys. Status Solidi (a)* 211 (2014) 1113–1121.
- [33] E. Zalnezhad, A. Hamouda, G. Faraji, S. Shamshirband, TiO₂ nanotube coating on stainless steel 304 for biomedical applications, *Ceram. Int.* 41 (2015) 2785–2793.
- [34] Q. Huang, Y. Yang, R. Hu, C. Lin, L. Sun, E.A. Vogler, Reduced platelet adhesion and improved corrosion resistance of superhydrophobic TiO₂-nanotube-coated 316L stainless steel, *Colloids Surf. B Biointerfaces* 125 (2015) 134–141.
- [35] K. Shankar, G.K. Mor, H.E. Prakasham, S. Yoriya, M. Paulose, O.K. Varghese, C.A. Grimes, Highly-ordered TiO₂ nanotube arrays up to 220 μm in length: use in water photoelectrolysis and dye-sensitized solar cells, *Nanotechnology* 18 (2007) 065707.
- [36] O.K. Varghese, D. Gong, M. Paulose, C.A. Grimes, E.C. Dickey, Crystallization and high-temperature structural stability of titanium oxide nanotube arrays, *J. Mater. Res.* 18 (2003) 156–165.
- [37] Q. Yao, C. Wang, B. Fan, H. Wang, Q. Sun, C. Jin, H. Zhang, One-step solvothermal deposition of ZnO nanorod arrays on a wood surface for robust superamphiphobic performance and superior ultraviolet resistance, *Sci. Rep.* 6 (2016) 35505.
- [38] B. Chen, J. Qiu, E. Sakai, N. Kanazawa, R. Liang, H. Feng, Robust and superhydrophobic surface modification by a “Paint + Adhesive” method: applications in self-cleaning after oil contamination and oil-water separation, *ACS Appl. Mater. Interfaces* 8 (2016) 17659–17667.
- [39] ASTM D3359-17 Standard Test Methods for Rating Adhesion by Tape Test, *ASTM International, West Conshohocken, PA*, 2017.
- [40] H. Ma, O. Acton, D.O. Hutchins, N. Cernetic, A.K.-Y. Jen, Multifunctional phosphonic acid self-assembled monolayers on metal oxides as dielectrics, interface modification layers and semiconductors for low-voltage high-performance organic field-effect transistors, *PCCP* 14 (2012) 14110–14126.
- [41] G. Zorn, I. Gotman, E. Gutmanas, R. Adadi, G. Salitra, C. Sukenik, Surface modification of Ti45Nb alloy with an alkylphosphonic acid self-assembled monolayer, *Chem. Mater.* 17 (2005) 4218–4226.
- [42] R. Hofer, M. Textor, N. Spencer, Alkyl phosphate monolayers, self-assembled from aqueous solution onto metal oxide surfaces, *Langmuir* 17 (2001) 4014–4020.
- [43] P. Kar, A. Pandey, J.J. Greer, K. Shankar, Ultrahigh sensitivity assays for human cardiac troponin I using TiO₂ nanotube arrays, *Lab Chip* 12 (2012) 821–828.
- [44] H.Z. Mohammad, F. Samira, D.W. Benjamin, A. Mohammad, M. Najia, K. Piyush, D. Mojgan, S. Karthik, Effect of phosphonate monolayer adsorbate on the microwave photoresponse of TiO₂ nanotube membranes mounted on a planar double ring resonator, *Nanotechnology* 27 (2016) 375201.
- [45] A. Mohammadpour, B.D. Wiltshire, Y. Zhang, S. Farsinezhad, A.M. Askar, R. Kisslinger, Y. Ren, P. Kar, K. Shankar, 100-fold improvement in carrier drift mobilities in alkanephosphonate-passivated monocrystalline TiO₂ nanowire arrays, *Nanotechnology* 28 (2017) 144001.
- [46] S. Pawsey, K. Yach, L. Reven, Self-assembly of carboxyalkylphosphonic acids on metal oxide powders, *Langmuir* 18 (2002) 5205–5212.
- [47] S. Rajendran, B. Apparao, N. Palaniswamy, A.J. Amalraj, M. Sundaravadivelu, The role of phosphonates as transporters of Zn²⁺ ions in the inhibition of carbon steel in neutral solutions containing chlorides, *Anti-Corros. Methods Mater.* 49 (2002) 205–209.
- [48] H.S. Awad, The effect of zinc-to-HEDP molar ratio on the effectiveness of zinc-1, hydroxyethylidene-1, 1 diphosphonic acid in inhibiting corrosion of carbon steel in neutral solutions, *Anti-Corros. Methods Mater.* 52 (2005) 22–28.
- [49] Z. Chu, S. Seeger, Superamphiphobic surfaces, *Chem. Soc. Rev.* 43 (2014) 2784–2798.
- [50] B. Bhushan, K. Koch, Y.C. Jung, Nanostructures for superhydrophobicity and low adhesion, *Soft Matter* 4 (2008) 1799–1804.
- [51] A. Cassie, Contact angles, *Discuss. Faraday Soc.* 3 (1948) 11–16.

- [52] V. Swamy, A. Kuznetsov, L.S. Dubrovinsky, R.A. Caruso, D.G. Shchukin, B.C. Muddle, Finite-size and pressure effects on the Raman spectrum of nanocrystalline anatase TiO₂, *Phys. Rev. B* 71 (2005) 184302.
- [53] G. Tompsett, G. Bowmaker, R. Cooney, J. Metson, K. Rodgers, J. Seakins, The Raman spectrum of brookite, TiO₂ (PBCA, Z = 8), *J. Raman Spectrosc.* 26 (1995) 57–62.
- [54] R. Luschtinetz, J. Frenzel, T. Milek, G. Seifert, Adsorption of phosphonic acid at the TiO₂ anatase (101) and rutile (110) surfaces, *J. Phys. Chem. C* 113 (2009) 5730–5740.
- [55] N. Kantor-Uriel, P. Roy, S. Saris, V. Kiran, D.H. Waldeck, R. Naaman, Evidence for enhanced electron transfer by multiple contacts between self-assembled organic monolayers and semiconductor nanoparticles, *J. Phys. Chem. C* 119 (2015) 15839–15845.
- [56] A. Ulman, *An Introduction to Ultrathin Organic Films: From Langmuir-Blodgett to Self-Assembly*, Academic Press, 2013.
- [57] M.H. Zarifi, S. Farsinezhad, B.D. Wiltshire, M. Abdorrazaghi, N. Mahdi, P. Kar, M. Daneshmand, K. Shankar, Effect of phosphonate monolayer adsorbate on the microwave photoresponse of TiO₂ nanotube membranes mounted on a planar double ring resonator, *Nanotechnology* 27 (2016) 375201.
- [58] L. Xu, Z. Geng, J. He, G. Zhou, Mechanically robust, thermally stable, broadband antireflective, and superhydrophobic thin films on glass substrates, *ACS Appl. Mater. Interfaces* 6 (2014) 9029–9035.
- [59] L.-H. Kong, X.-H. Chen, L.-G. Yu, Z.-S. Wu, P.-Y. Zhang, Superhydrophobic cuprous oxide nanostructures on phosphor-copper meshes and their oil-water separation and oil spill cleanup, *ACS Appl. Mater. Interfaces* 7 (2015) 2616–2625.